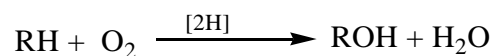


Concluding remarks

The importance of 6-substituted pterins, especially their reduced forms for the functioning of different classes of redox metalloenzymes, is well-known. Nature has achieved optimum synchronization among the changes in oxidation levels of the substrate, the concerned metal centre and the pterin/pyrazine ring in such cases. With this view in mind the coordination chemistry of a 6-substituted pterin ligand has been pursued here with the bivalent transition metal ions like Co(II), Ni(II), Cu(II) and Zn(II). Bench mark data (characterization, spectroscopic, physico-chemical and reactivity) have been recorded for the new coordination compounds. Although a significant portion of the data is concerned with compounds involving the oxidized (aromatic) form of the pterin ligand with a bivalent metal centre, attempts have been made to access the lower oxidation state of the metal ion in suitable cases [e.g., Co(I), Ni(I), Cu(I)] in presence of a partly reduced form (e.g., the 7, 8-dihydro state, L^{2-}) of the ligand. The concerned Frost diagram (Scheme IV-11) predicts only a small thermodynamic barrier ($\Delta G^\circ = -NFE^\circ$) for the transformation $M(II) \rightarrow M(I)$ ($M = Co, Ni, Cu$), with the associated kinetic step being achieved here without much difficulty. The pyrazine ring of the pterin ligand, is the locant of reducing equivalent storage/transfer; pure compounds containing both a M(I) metal centre and a reduced form (7, 8-dihydro pterin) of the ligand, could be obtained using $NaBH_4$ reduction. Some of the labile intermediates in between the above two extremes (i.e., the fully oxidized and fully reduced forms of these complexes) could be visualized on the time scales of cyclic voltammetry and also from the reaction profiles followed using UV-VIS spectroscopy; the relative intensities of fluorescence spectral bands are a good measure of the electron densities (oxidation states) of the pterin rings in the new complexes. Interesting results have been obtained from the reactivity studies on the reduced forms of these compounds as well as their formation

from the corresponding oxidized forms. They throw light not only on the different facets of redox chemistry of pterin compounds but also helpful in understanding the reaction catalyzed by phenylalanine hydroxylase (PAH).

Scheme I-13 summarizes the PAH catalytic cycle where the tetrahydrobiopterin cofactor (BH₄) plays a decisive role in transferring reducing equivalents to the phenylalanine/O₂ reaction system, itself being oxidized to BH₂ during this step; NADH restores the reduced state (BH₄) once again. Two chemically significant steps associated with this process are: (i) the activation of the dioxygen (O₂) molecule and (ii) the activation of the aromatic ring (of the substrate) towards hydroxylation.

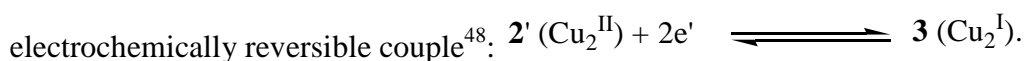


The present new compounds provide with a scope for understanding some of the above aspects.

Copper-pterin chemistry has been explored in chapter II which has several important features.

The fact that [Cu^{II}(L)(phen)(H₂O)]. 3H₂O (**2**) could be synthesized by three different routes, is a sufficient indication of its chemical/ thermodynamic stability. Formation of **3** from **2** by NaBH₄ reduction as well as its characterized by different methods including 2D NMR (¹H-¹H COSY) is interesting; the latter step verifies **3** to be a Cu(I) complex with a reduced form [(L⁻²⁻), 7, 8-dihydro pterin] of the pterin ligand (Scheme II-5 and II-6). From the kinetic data (Figure II-23) as well as thermodynamic considerations, it is evident that the formation of **3** is a two-step process (Scheme II-6); but **3** is able to transfer its reducing equivalents to the bromobenzene/O₂ reaction mixture in a single step (Figure II-25; Scheme II-7 and II-8).

For the quasi-reversible cyclic voltammetric data of **3** [Figure II-20(b)], the cathodic (E_{pc}) and anodic (E_{pa}) responses can be interpreted in terms of the forms **3** and **2'** as shown in Scheme II-6; the i_{pc}/i_{pa} ratio (0.97; Table II-6) indicates sufficient kinetic stability for the intermediate binuclear species **2'** on the cyclic voltammetric time scale as well as the existence of the



The above cathodic and anodic steps can be correlated with the chemical redox processes as shown in Figure II-23(b) (NaBH₄ reduction) and Figure II-25 (oxidation by O₂/bromobenzene reaction mixture) respectively. Presence of isosbestic points is a common feature of these two chemical steps, indicating single-step conversions.

Figure II-27 summarizes the above aspects and at the same time throws light on the mechanism of hydroxylation of bromobenzene by **3** in presence of O₂. Possibly, the formation of a **3**(O₂) complex initiates the process, followed by concerted electron transfer **3**→O₂ and reducing equivalent transfer from the 7, 8-dihydro form of the pterin ligand (L') to the reaction system; sufficient stability of **2** ensures completion of the last step. The exceptionally small band gaps (0.5 eV) for some of the frontier orbitals of **2** and **3**, play a vital role in controlling such electron/reducing equivalent transfers. As the direct transfer of reducing equivalents from NaBH₄ to the bromobenzene/O₂ reaction mixture is not possible, the **2/3** combination may be regarded as a model mediator for this purpose.

Chapter III is concerned with cobalt-pterin chemistry where the mixed ligand compound [Co^{II}(L)(phen)(H₂O)]. 3H₂O (**2**) plays a vital role in elucidating redox properties. On reduction with NaBH₄ in CH₃OH it affords Na[Co^I(L')(phen)(H₂O)]. 2H₂O.CH₃OH (**3**), where (L')²⁻ = 7, 8-dihydro form of the pterin ligand (L)²⁻. Magnetic susceptibility and other physico-chemical data indicate **2** and **3** to be high-spin Co(II) and Co(I) complexes, respectively. Frost diagram

(Scheme IV-11) predicts a facile $\text{Co(II)} \rightarrow \text{Co(I)}$ conversion which could be visualized in cyclic voltammetry as an irreversible reduction peak at -0.6V . Such reduction process is accompanied by a considerable increase in fluorescence emission intensity. The corresponding chemical reduction process by NaBH_4 can be followed UV-VIS spectroscopically (Figure III-13) where the presence of isosbestic points indicates the conversion $\mathbf{2} \rightarrow \mathbf{3}$ to be a one-step process. Such data are consistent with the chemical composition of $\mathbf{3}$, indicating a mononuclear species with Co(I) centre and a reduced form (L') of the pterin ligand. On the other hand, the reaction profile (Figure III- 14) representing the transfer of reducing equivalents from $\mathbf{3}$ towards the $\text{O}_2/\text{bromobenzene}$ reaction mixture, is devoid of any isosbestic point. It provides with a much-needed information about the mechanism of hydroxylation of bromobenzene here. Formation of a dioxygen complex $\mathbf{3}(\text{O}_2)$ most likely initiates this reaction which is followed by sequential transfer of electron ($\text{Co}^{\text{I}} \rightarrow \text{Co}^{\text{II}} + \text{e}'$) to O_2 and reducing equivalents from the 7, 8-dihydro pterin ligand moiety (L') to the reaction system, achieving bromobenzene \rightarrow 4-bromophenol conversion. The remarkably small band gaps ($<0.5\text{eV}$) for the frontier orbitals of $\mathbf{2}$ and also for a few of $\mathbf{3}$ (Figure III-17) are helpful in controlling such facile electron/reducing equivalent transfers towards $\mathbf{2}$ or out of $\mathbf{3}$ respectively.

Chapter IV focuses its attention on the two new mixed ligand Ni(II) complexes, e.g., $[\text{Ni}^{\text{II}}(\text{L})(\text{en})(\text{H}_2\text{O})] \cdot 2\text{H}_2\text{O}$ ($\mathbf{1}$) and $[\text{Ni}^{\text{II}}(\text{L})(\text{en})(\text{Im})] \cdot 2\text{H}_2\text{O}$ ($\mathbf{2}$), for pursuing nickel-pterin chemistry. In terms of chemical compositions and molecular structures, only an imidazole ligand distinguishes $\mathbf{2}$ from $\mathbf{1}$; but it has a profound effect on the redox reactivity profiles. Here the 'en' chelate ring possesses a δ -conformation and the extent of such puckering may be assessed from the CD spectral data of $\mathbf{1}$ and $\mathbf{2}$.

Only a small thermodynamic barrier (Frost diagram, Scheme IV-11) is associated with the conversion Ni(II) \rightarrow Ni(I) and NaBH₄ reduction in CH₃OH helps to achieve it, providing **1R** and **2R** from **1** and **2** respectively, accompanied by a significant fluorescent emission intensity increase. Both **1R** and **2R** have been characterized as mononuclear mixed ligand Ni(I) complexes of 7, 8-dihydro form of the pterin ligand (L'), with 'en' as the ancillary ligand. The quasi-reversible ($\Delta E_p = 75 - 188$ mV) cyclic voltammetric responses of both **1** and **2**, are helpful in visualizing the Ni(II)/Ni(I) states here.

A comparison of reaction profiles (Figure IV-30 and IV-31) for the interaction of K₃[Fe(CN)₆] with NaBH₄ and **2R** respectively, is quite interesting. While K₃[Fe(CN)₆] is essentially unable to accept reducing equivalents from NaBH₄ directly, the reverse is true for **2R**; presence of isosbestic point for the latter process indicates a single-step conversion. In other words, the **2/2R** combination serves here as an excellent mediator (Scheme IV-14) of reducing equivalents between NaBH₄ and K₃[Fe(CN)₆].⁹⁴ The same property is manifested during the reactions of **1** and **2** with NaBH₄ and those of **1R** and **2R** with the bromobenzene/O₂ reaction mixture. The reaction profiles (Figure IV-24 and IV-27) representing the reduction **1** \rightarrow **1R** and the transfer of reducing equivalents from **1R** to the bromobenzene/O₂ mixture, are devoid of any isosbestic points, hinting at multistep processes. But those for **2** and **2R** (Figure IV-28 and IV-29) possess such an attribute, indicating single-step conversions, commensurate with the chemical composition of **2R** (i.e., a mononuclear species). Such flexible redox behavior of **1** and **2** can be traced to the small band gaps (<0.5 eV) for some of their frontier orbitals (Figure IV-32).⁶⁴⁻⁶⁶

The most-interesting aspect of this study is that the control of reducing equivalent mediator property of a nickel-pterin centre by a donor atom from an ancillary ligand; viewed in

the context of a metalloprotein or metalloenzyme, such control of function of a metal-centred cofactor, is achieved by donor atoms from the anchoring protein chain.

Chapter V delves deeper into nickel-pterin chemistry using two new chiral Ni(II) complexes (**2** and **3**) with the identical chemical composition $[\text{Ni}^{\text{II}}(\text{L})(\text{pn})(\text{H}_2\text{O})] \cdot 5\text{H}_2\text{O}$; here 'pn' stands for the two chiral ancillary ligands R-(+)-1,2-diaminopropane [R-(+)-pn] and S-(-)-1,2-diaminopropane [S-(-)-pn] respectively. X-ray structural data establish δ -conformation for the 'pn' chelate ring in each case, but for **3** the extent of such distortion is more significant, approaching near planarity. Such conformational difference between **2** and **3** induced by the R-(+)-pn and S-(-)-pn chelate rings, affect their reactivities considerably; even their crystal packing diagrams/H-bonding networks are different (Figure V-3 and V-5). The effect of H-bonding on the redox properties of biomolecules is well-known¹⁶².

The Ni(I) state of both **2** and **3** could be accessed in terms of their quasi-reversible cyclic voltammetric responses ($\Delta E_p = 138 - 153 \text{ mV}$) (Figure V-17 and V-18). NaBH_4 reduction in CH_3OH affords the reduced forms of **2** and **3**, i.e., **2R** and **3R** respectively; analytical data indicate them to be mononuclear Ni(I) complexes with the 7, 8-dihydro form of the pterin ligand (L'). The reaction profiles representing the interactions of NaBH_4 with **2** and **3** (Figure V-21 and V-22) highlight the conformational control of redox reactions in terms of the absence or presence of isosbestic points, affecting both the metal and pterin ligand centres. The products of such reactions, i.e., **2R** and **3R** transfer their reducing equivalents to a typical electron acceptor like $\text{K}_3[\text{Fe}(\text{CN})_6]$ through pathways having subtle differences (Figure V-23 and V-24). Difference in kinetic parameters (Table V-6) are also observed for the transfer of reducing equivalents from **2R** and **3R** to the bromobenzene/ O_2 reaction mixture.

The 'pn' chelate ring conformational differences affect the electronic structures of **2** and **3** as well. For example, a small band gap (< 0.5 eV) exists between the HOMO and (HOMO-1) levels of **2**; on the other hand such a small band gap is observed for **3** between the (LUMO+1) and LUMO levels (Figure V-26). In other words, the conformational and electronic structural differences act synergistically, for achieving such reactivity differences between **2** and **3**.

The implicit bioinorganic significance (vis-à-vis the metalloenzymes) of the above conformational control of redox properties (or reducing equivalent transfer properties) of nickel-pterin centres by the ancillary ligand chelate rings, may be understood¹⁰⁰.

Finally, chapter VI focuses its attention on four mononuclear mixed ligand complexes (**1** – **4**) of bivalent transition metal ions [Co(II), Ni(II), Cu(II) and Zn(II)], with 2,2'-bipyridyl acting as the ancillary ligand in three cases. The x-ray structural, spectroscopic and electrochemical data of the complex compound with redox silent Zn(II) centre (**1**), play a crucial role here in substantiating some of the interpretations presented in earlier chapters. For example, the multiple nature of the NH₂(2) – C(2) and C(4) – O(4) bonds [C13 – N17, 1.335(3)Å and C15 – O16, 1.257(3)Å in Figure VI-1] verifies that the electron-shuffling of the pterin ring (L²⁻) is essentially responsible for such observations, with little participation from the metal centre.

This Zn(II) complex (**1**) possesses an intense ($\log \epsilon = 4.086$) electronic spectral band at 733 nm (Figure VI-14) which can only be ascribed to a MLCT band Zn(II)(d¹⁰) e_g* \rightarrow π^* (phen). Such long wavelength intense bands are common features of the Co(II), Ni(II), Cu(II) complexes discussed earlier and they could be interpreted using suitable MO diagrams. The frontier orbitals (Figure VI-31 and VI-32) of **1** – **4** are characterized by at least a couple of band gaps which are remarkably small (< 0.5 eV), conferring unique redox properties on them.⁶⁴⁻⁶⁶ For **1** the HOMO \rightarrow LUMO transition is essentially a pterin \rightarrow phen electron transfer through the Zn(II)(d¹⁰) centre

(Figure VI-31) or an internal redox process covering the entire molecule. This is consistent with the π -acidic nature of the 'phen' ligand; it is further verified by the ^1H NMR spectrum (Figure VI-23 and Scheme VI-8) of **1** where the 'phen' protons undergo shielding through coordination with the Zn(II) centre. The cyclic voltammogram of **1** (Figure VI-26) lacks any cathodic reduction peak (Epc) over the range -0.6V to -0.8V; this observation may be linked to the redox silent nature of the concerned metal centre [Zn(II)]. The fluorescence and EPR spectral data as well as the reactivity studies presented here, augment the inferences of earlier chapters.

Active site of the heme proteins/enzymes like Hb/Mb, cytP-450 and cyt c describe almost graphically how the same cofactor (iron-porphyrin) can be modulated for different purposes (ranging from oxygen carrier to electron carrier as well as monooxygenase activity) through selective coordination by donor atoms from the anchoring protein chain.

Such level of understanding about the structural control of function is yet to be achieved for the pterin-containing metalloenzymes.

Synthetic, physico-chemical and reactivity studies on new model coordination compounds, provide with suitable pathways for achieving such research goals. The present work is a sincere attempt in that direction.

References

- (1) Hille, R. *Chem. Rev.* **1996**, *96*, 2757 – 2816.
- (2) Johnson, M. K.; Rees, D. C.; Adams, M. W. W. *Chem. Rev.* **1996**, *96* 2817 – 2840.
- (3) Enemark, J. H. ; Cooney, J. J. A. ; Wang, J. J. ; Holm, R. H. *Chem. Rev.* **2004**, *104*, 1175 – 1200.